Full-Body Compliant Human–Humanoid Interaction: Balancing in the Presence of Unknown External Forces

Sang-Ho Hyon, *Member, IEEE*, Joshua G. Hale, and Gordon Cheng, *Senior Member, IEEE*

***Abstract*—This paper proposes an effective framework of human–humanoid robot physical interaction. Its key component is a new control technique for full-body balancing in the presence of external forces, which is presented and then validated empirically. We have adopted an integrated system approach to develop humanoid robots. Herein, we describe the importance of replicating human-like capabilities and responses during human–robot interaction in this context. Our balancing controller provides gravity compensation, making the robot passive and thereby facilitating safe physical interactions. The method operates by setting an appropriate ground reaction force and transforming these forces into full-body joint torques. It handles an arbitrary number of force interaction points on the robot. It does not require force measurement at interested contact points. It requires neither inverse kinematics nor inverse dynamics. It can adapt to uneven ground surfaces. It operates as a force control process, and can therefore, accommodate simultaneous control processes using force-, velocity-, or position-based control. Forces are distributed over supporting contact points in an optimal manner. Joint redundancy is resolved by damping injection in the context of passivity. We present various force interaction experiments using our full-sized bipedal humanoid platform, including compliant balance, even when affected by unknown external forces, which demonstrates the effectiveness of the method.**

***Index Terms*—Balance, biped robot, compliance, force control, full-body motion control, human–humanoid interaction, passivity, redundancy.**

I. Introduction

THE adaptation of the human environment to suit human sensory and motor capabilities necessitates artificial agents with analogous capabilities that can usefully coexist in our living and working spaces. Humanoid agents can take further advantage of the multipurpose adaptability of the human form itself for performance of a broad range of activities. Such activities might include cooperating with humans themselves, so that humanoid robots benefit not only from suitability of the human form in an individual context but also through its impact on the relationship between humans and robots. For example, the appearance of a human induces an expectation of human-like responses [1]–[3]. Besides its scientific benefits [4], the most appropriate form for a robot acting as a partner for a human is a humanoid of human proportions [5]. Having similar physical capabilities, a human-like presence and the use of familiar social cues make cooperation natural because it is intuitively easier to relate to the following: experience of interaction with other humans trains people to accommodate basic factors such as their partner's balance, range of motion, working space, physical intentions, etc. [6], [7]. Human imitation is, therefore, of increasing importance: human-like behavior, emotionally and aesthetically pleasing action, and expressive motion are fundamental. In addition, according to the logic that a tool inherently enhances the way we think, humanoid robots increase our understanding of human behavior, and consequently, our intellectual abilities [8], [9].

The persistent and increasingly difficult problem for the design of appropriate intelligent systems is, therefore, *how* to communicate and cooperate with people. Physical interaction is a familiar and reliable method for most humans; it encompasses both physical cooperation and communication through movement. This motivates an exploration of physical interactions between humans and robots. Physical interaction can encourage people to perceive and respond to a robot as a human-like being rather than as a mechanical entity [10], thereby prompting ways of making robot–human interactions more natural.

For the discussions included in this paper, we regard such activities as high-level motion planning that might be conceived of as subsystems in an integrated view of a humanoid robot system [9], [11]. We rather present a motion subsystem for balancing that exemplifies the interaction and compatibility espoused by the integrated model. The conceptual organization is illustrated in Fig. 1.

A. Balancing

The need for a balancing system arises from the requirement that the humanoid be capable of performing on a similar level as that of humans. Human-sized robot bipeds are constrained by severe restrictions on force interactions because of the requirements of bipedal balance. To facilitate continuous interaction with its environment and with people, a bipedal robot must be able to maintain balance in a manner that accommodates external forces. We are interested in a force-controlled balancing

Manuscript received October 16, 2006; revised May 22, 2007. This paper was recommended for publication by Associate Editor C. Laschi and Editor H. Arai upon evaluation of the reviewers' comments. This work was supported by the Keihanna branch of the National Institute of Communication Telecommunication (NiCT), Japan.

The authors are with the Japan Science and Technology (JST), International Cooperative Research Project (ICORP), Computational Brain Project, Saitama 332-0012, Japan. They are also with the Computational Neuroscience Laboratories, Advanced Telecommunications Research Institute International (ATR), Kyoto 619-0288, Japan (e-mail: sangho@atr.jp; jhale@atr.jp; gordon@atr.jp).

This paper has supplementary downloadable material available at http://ieeexplore.ieee.org, provided by the authors. This includes a single multimedia MPEG4 format video, which show the experimental results. This material is 10 MB in size.

Digital Object Identifier 10.1109/TRO.2007.904896

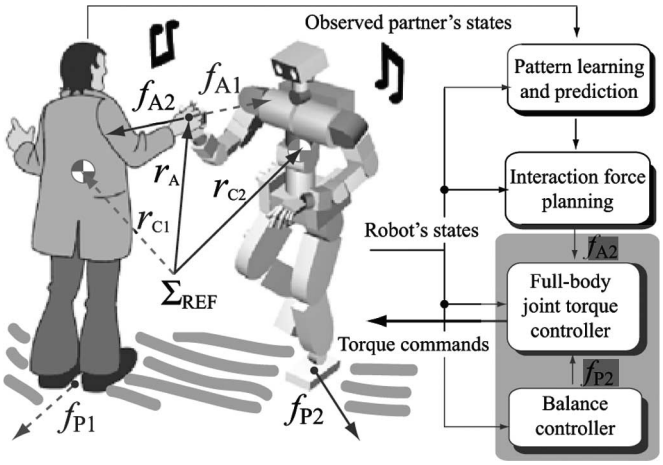

Fig. 1. Possible control flow in force interaction with balance. Shaded region is described in the text: how to generate full-body joint torques for given interaction forces: f_{A2} and f_{P2}. The gross motion of the robot r_{C2} reflects both the control action (joint torque) and the interaction force f_{A1} applied by the human.

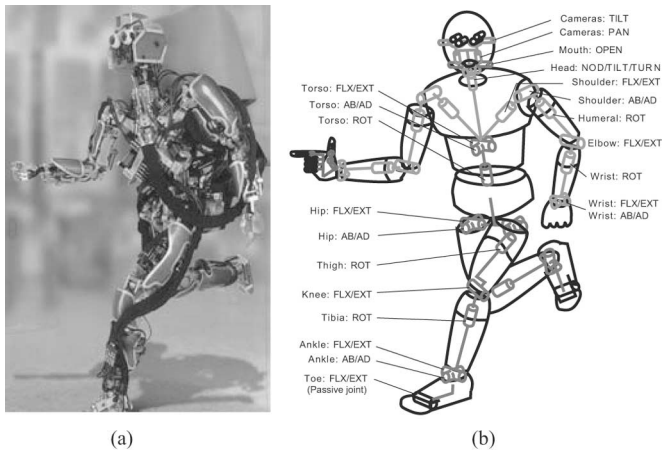

Fig. 2. New torque-controllable biped humanoid robot *CB* developed by SARCOS. (a) Hardware. (b) DoF configuration.

system, reasoning that: 1) force control is a superset containing velocity-based and position-based control that enables adoption of any of these strategies, thereby allowing for the richest level of physical communication, and 2) force interaction is a familiar and reliable method for physical communication and cooperation with humans. In addition, the force-controlled system renders our system compliant: interaction with humans is both feasible and safe.

The activity shown in Fig. 1 illustrates the control flow during a force interaction with a human: dancing. In such a force interaction task, two levels are distinct within the control process: 1) designing the interaction forces and 2) generating the joint torques. The first process computes the required interaction forces f_{A2} in accordance with the given task while considering the self-balancing force f_{P2}, which acts on the environment. The latter determines the joint torques for the full body that are necessary to produce the interaction forces. This paper particularly describes issues related to the latter control process, which is indicated as the shaded region in Fig. 1. Specifically, this paper provides a theoretical foundation for bipedal balancing with force interactions. We address the following issues that arise during force interactions between humans and bipedal humanoid robots with multiple degrees of freedom (DoFs):

i) How to maintain self-balance.
ii) How to cope with external forces.
iii) How to handle redundant DoF.

Historically, issues (I1) and (I2) have mainly been pursued in the field of bipedal walking robots. Several balancing compensators have been developed for position-controlled bipedal humanoids. Some position-based balance compensators have been successful [12]–[16].

However, position-based controllers cannot quickly adapt to sudden environmental changes, especially to unknown external forces. That insufficiency is an important disadvantage for position-based controllers in terms of *force interaction*. First, the methods require force measurement. Second, time delays caused by the recalculation of the joint trajectories are unavoidable. Third, and most problematically, it is difficult to assign appropriate weights in the presence of unknown disturbances. See Section V for details.

In our prior study [17], to avoid the complex motion planning that is required for multi-DoF bipedal walking, we applied position-based compliance control so that a robot adapts compliantly to external forces by using a force sensor. Such methods, however, can deal only with forces via *virtual* compliance; for that reason, time delays are, in principle, unavoidable. Moreover, the controller requires force sensors at *every* expected contact point. Without them, the robot cannot adapt to unknown external forces. Although it is possible to install force sensors over the whole body, this imparts a heavy computational burden because of the number of contact Jacobians. We, therefore, have inferred that the best way to treat unknown disturbances and external forces is to transform desired contact (interaction) forces into joint torques directly, even though controlling these joint torques precisely is technically challenging.

B. Contribution and Organization of This Paper

The contribution of this paper is the presentation of a simple and practical method of force interaction control addressing issues (I1)–(I3). Specifically, we propose a passivity-based, full-body, contact force controller, and apply it to force interaction between humans and dynamically balancing bipedal humanoid robots. Unlike previous methods, the controller can accommodate an arbitrary number of contact forces; it requires no force sensors at the contact points. We experimentally evaluate the controller on our new biped humanoid platform (Fig. 2) developed by SARCOS (www.sarcos.com). This robot has 50 DoF and torque controllability, which we have been pursuing during hardware and software development over the past several years [4], [5]. We highlight our work with various demonstrations of simultaneous force interaction with humans, and bipedal balance maintenance. In particular, we demonstrate that the robot can adapt to *unknown* external forces applied to *arbitrary* contact points *without sensing* the contact forces.

The paper is organized as follows. Section II describes our passivity-based full-body force control framework [18], where we specifically examine how to compute the commanded joint torque for a given desired contact force. The proposed method is novel with respect to two major points: 1) it is applicable to redundant DoF humanoid robots and 2) it is applicable to multiple contact points, even when they form a closed-loop chain. The former novelty is attributable to passivity-based redundancy resolution, which requires neither a contact-force measurement, nor inverse kinematics/dynamics. The latter novelty comes from an optimization of contact forces in terms of the L_2 norm of the contact forces, avoiding unnecessary internal forces between the contact points. Gravity compensation, which is widely used in position control of manipulator, is highlighted in the context of the full-body-contact force control framework [19]. Gravity compensation is extremely useful for physical interaction between humans and humanoids because the robot's movement can thereby be controlled using very small external forces. Specific methods for force interaction with balance are described in Section III, where simple controllers and simulations are proposed. Section IV describes various balanced force-interaction experiments on our humanoid platform. The experiments include balancing with unknown external forces, adaptation to different contact points. The experimental results are supplemented with a video included with this paper, which is available at http://ieeexplore.ieee.org.[1] Section V presents a comparison of the proposed method with other related methods. Finally, Section VI summarizes the results from human–robot interaction perspective and presents discussion of future work.

II. Passivity-Based Full-Body Force Control Framework

Bipedal humanoid robots must maintain their balance through contact forces while interacting with the environment. For the study described in this paper, we assume that the central issue for force interaction between humans and bipedal humanoid robots is the control of contact forces. This section presents a new force control framework for humanoids with multiple contact points and multiple force interaction points [18]. First, Section II-A derives *ground applied force* (GAF; see the definition therein) from the full nonlinear dynamics of the robot. Then, Section II-B shows how to transform the desired GAF to joint torques without using inverse kinematics or inverse dynamics. The key technology is gravity-compensation and passivity-based redundancy resolution. Also, Section II-C explains how to distribute the GAF to multiple contact points. Finally, Section II-D summarizes the preceding descriptions and provides the control procedure.

A. Dynamics of Multi-DoF Humanoid and the GAF

Consider a multi-DoF humanoid robot contact with the ground, as shown in Fig. 3. Let $r \in \mathcal{R}^3$ in Σ_W be some translational position coordinate (e.g., base position) and $q \in \mathcal{R}^n$ be the joint angles *and* attitude of the base. Using the generalized coordinates $\hat{q} = [r,\ q]^T \in \mathcal{R}^{3+n}$, the exact nonlinear dynamics of humanoids with the constraint can be derived using a standard Lagrangian formulation with constraints [20]

$$\hat{I}(\hat{q})\ddot{\hat{q}} + \hat{C}(\hat{q}, \dot{\hat{q}}) + \hat{G}(\hat{q}) = u + E(\hat{q})^T \lambda \tag{1}$$

$$E(q)\dot{\hat{q}} = 0 \tag{2}$$

where $\hat{I}(\hat{q}) \in \mathcal{R}^{(3+n)\times(3+n)}$ is the inertia matrix, $\hat{C}(\hat{q}, \dot{\hat{q}}) \in \mathcal{R}^{3+n}$ respectively represent the centrifugal and Coriolis terms, $\hat{G}(\hat{q}) \in \mathcal{R}^{3+n}$ is the gravity term, $u = [0,\ \tau]^T \in \mathcal{R}^{3+n}$ is the generalized forces, $E(q) \in \mathcal{R}^{3\times(3+n)}$ is the constraint Jacobian associated with the contact, and $\lambda \in \mathcal{R}^3$ is the constraint force. First, we assume that at least one point of the sole is contacting with the ground. For simplicity, we specifically examine the single holonomic constraint. We will discuss the multiple contact case in Section II-C.

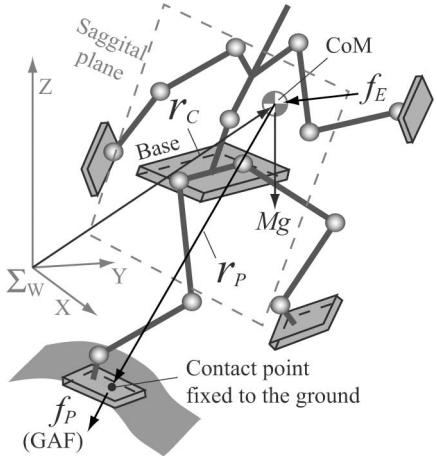

Fig. 3. Coordinate definition.

Our important control issue described in this paper is balancing. Therefore, it is convenient to address the center of mass (CoM) coordinate. Let $r_C = [x_C,\ y_C,\ z_C]^T \in \mathcal{R}^3$ be the position vector of CoM in the world coordinate frame. Also, let Σ_W and $r_P = [x_P,\ y_P,\ z_P]^T \in \mathcal{R}^3$ be the position vector from CoM to the contact point (see Fig. 3). The contact point does not move on the ground surface. For convenience, we introduce a *gross applied force*, or *GAF* $f_P = [f_{xP},\ f_{yP},\ f_{zP}]^T$, defined as $f_P := -f_R$, where f_R is the ground reaction force (GRF). Herein, GAF represents the force that the robot applies to the environment through the contact point. The control objective of the contact force control is to bring f_P to some desired value $\bar{f}_P$.

By replacing the generalized coordinates $\hat{q}$ with $\hat{q}_C = [r_C,\ q]^T \in \mathcal{R}^{3+n}$, (1) is converted to the decoupled dynamics:

$$\underbrace{\begin{bmatrix} M & 0 \\ 0 & I(q) \end{bmatrix}}_{\hat{I}} \underbrace{\begin{bmatrix} \ddot{r}_C \\ \ddot{q} \end{bmatrix}}_{\ddot{\hat{q}}_C} + \underbrace{\begin{bmatrix} 0 \\ C(q,\dot{q}) \end{bmatrix}}_{\hat{C}} + \underbrace{\begin{bmatrix} -Mg \\ 0 \end{bmatrix}}_{\hat{G}} = \underbrace{\begin{bmatrix} 0 \\ \tau \end{bmatrix}}_{u} - \underbrace{\begin{bmatrix} id \\ J_P(q)^T \end{bmatrix}}_{\hat{E}(q)^T} f_P \tag{3}$$

[1]This is a single MPEG4 format movie that shows the empirical results. The movie is 10 MB in size. For details, see "readme.txt" in the same file directory.

$$\hat{E}(q)\dot{\hat{q}}_C = 0 \tag{4}$$

wherein $M = \mathrm{diag}(m, m, m) \in \mathcal{R}^{3\times 3}$ is the mass matrix (m is the total mass), $I(q) \in \mathcal{R}^{n\times n}$ is the inertia matrix, $C(q, \dot{q}) \in \mathcal{R}^n$ is the centrifugal and Coriolis term, $id \in \mathcal{R}^{3\times 3}$ denotes the identity matrix, and $J_P(q) \in \mathcal{R}^{3\times n}$ is the Jacobian from CoM to the contact point (derivative of r_P with respect to q). The Jacobian $J_P(q)$ can be derived easily using a standard kinematics computation (see [21, Sec. 3.1.3] for example). Note that (4) is the time derivative of the holonomic constraint $r_C + r_P = \text{constant}$ (see Fig. 3). The upper part of (3) portrays simple linear dynamics:

$$M\ddot{r}_C = Mg - f_P. \tag{5}$$

Consequently, we can control $\ddot{r}_C$ by f_P, as we will show in Section III-A.

Differentiating (4) yields

$$\hat{E}(q)\ddot{\hat{q}}_C + \gamma(q, \dot{q}) = 0 \tag{6}$$

where $\gamma(q, \dot{q}) = (\partial/\partial q_C)(\hat{E}\dot{q}_C)\dot{q}_C$. Solving (3) and (6) for $\ddot{\hat{q}}_C$ yields

$$f_P = (\hat{E}\hat{I}^{-1}\hat{E}^T)^{-1}\{\gamma + \hat{E}\hat{I}^{-1}(u - \hat{C} - \hat{G})\}. \tag{7}$$

Therefore, for some desired GAF $\bar{f}_P$, we can calculate the corresponding joint torques τ by inverting (7). The torque precisely achieves $f_P = \bar{f}_P$ as long as the earlier model is correct (model parameters and sensor measurements). We have considered only one contact point. The single contact point is exactly the center of pressure (CoP) if no other contact points exist. In this case, the robot is *underactuated* because the robot cannot generate the moment around the contact point, and the first three entries in τ become zero. Inverse dynamics are useful for this case. See [22] for more details of this type of exact GAF control. Usually, inverse dynamics control becomes impractical for robots with many DoFs. In addition, even if the inverse dynamics have been calculated successfully, we must yet solve the redundancy problem. When there are multiple contact points, it remains unclear how to resolve the contact forces because many possible solutions exist, which is well known as an ill-posedness problem in the field of robotic grasp (see, for example, [23] and [24]). The following two sections specifically address these issues.

B. Calculating Commanded Joint Torque With Gravity Compensation

The problem here is how to transform the desired GAF into joint torques "effectively." We intend to avoid exact inverse dynamics calculation because it requires an exact model including the inertia matrix, which becomes impractical for large-DoF systems. Second-ordered velocity terms are especially problematic because the velocity measurement is usually noisy. On the other hand, the gravity term is readily identifiable and a dominant nonlinear term in full dynamics. For that reason, G-comp plays a central role in contact force control.

This point is clarified if we assume that the motion is quasi-static. We assume that the robot foot fully contacts with the ground. Therefore, the first three entries in τ are available, that is, the robot is *fully actuated*. In this case, $\dot{q} \approx 0$; therefore, $\gamma \approx 0$, $\hat{C} \approx 0$ hold. For some new force input $f_u = [f_{ux},\ f_{uy},\ f_{uz}]^T \in \mathcal{R}^3$, it is straightforward that the joint torque

$$\tau = J_P^T(f_v + Mg) \tag{8}$$

$$f_v = f_u + (J_P I^{-1} J_P^T)^{-1} M^{-1} f_u \tag{9}$$

renders the closed-loop system satisfying

$$f_P \approx f_u + Mg. \tag{10}$$

See Appendix I for the proof. This is the main idea of G-comp for controlling contact forces. Consequently, we obtain $M\ddot{r}_C \approx -f_u$. That is, we can control the CoM movements using f_u.

In (9), we used the inertial matrix $I(q)$, which might be difficult to obtain in some applications. A simpler formula is available by setting

$$\tau = J_P^T(f_u + Mg) \tag{11}$$

that is, $f_v := f_u$, instead of (8) and (9). This approximation is valid whenever $f_u = 0$ (G-comp only) or f_u is given by some feedback law. We assume that this is true for all range of the motion. If the posture is singular, this coefficient becomes very large, and (10) does not hold unless $f_u = 0$.

On the other hand, the static force control for *redundant* manipulators is well known to cause *internal motions* [23]. Some dynamic effects might arise as the internal motions if γ and C are not small. We must, therefore, compensate for the internal motion somehow, while simultaneously achieving a desired GAF. One simple way to accomplish these requirements is to assign a simple nonlinear term that compensates γ and C. Substituting (8) and $(\partial/\partial q)(J_P\dot{q})\dot{q} = -J_P\ddot{q}$ into (7), we can derive a modified version of (8)

$$\tau = J_P^T\,(f_v + Mg) + \zeta(q, \dot{q}) \tag{12}$$

which yields convergence of the GAF

$$f_P \to f_u + Mg\ (t \to \infty) \tag{13}$$

provided $\zeta(q, \dot{q})$ is designed so that

$$I(q)\ddot{q} + C(q, \dot{q}) - \zeta(q, \dot{q}) = 0 \tag{14}$$

is stable. The proof is available in Appendix II. A conservative means to achieve this is simply to set ζ as joint-wise damping

$$\zeta = -D\dot{q} \tag{15}$$

with a constant diagonal matrix $D > 0$. Although we should investigate the structure of the left-hand side of (14), the controller (12) itself can be made very simple, as in this example. See [25] and [26] for a damping injection strategy for controlling redundant manipulators, where the authors analyzed the convergence of the internal motions and the position error of the end-effector.

The closed loop system (3) + (12) becomes

$$M\ddot{r}_C = -f_u - f_\zeta + f_E \tag{16}$$

$$I(q)\ddot{q} + C(q, \dot{q}) = J_P(q)^T f_v + \zeta(q, \dot{q}) \tag{17}$$

where f_ζ is the dissipation term associated with the third term of (12). As a result, we obtain the *passivity* [27], [28] relationship

$$H(q,\dot{q}) := \frac{1}{2}\dot{r_C}^T M \dot{r_C} + \frac{1}{2}\dot{q}^T I \dot{q} = \frac{1}{2}\dot{q}^T (J_P^T M J_P + I)\dot{q} \leq \int f_v^T J_P(q)\dot{q}\, dt + \int f_E^T J_P(q)\dot{q}\, dt. \quad (18)$$

Consequently, we have the following properties.

1) CoM tracking is possible with the addition of simple controllers using f_u as in Section III-A.
2) Without external forces f_E, the CoM is subject to the constant velocity movement.
3) Without user forces f_u, the CoM and *all* the joint movements can be driven externally by f_E.

The third one is particularly useful for safe force interaction. For example, humans can escort the robot in an arbitrary direction by pulling its hand. Alternatively, humans can teach dancing movements by holding and moving arbitrary segments of the body if balancing is coordinated automatically by the controller described in Section III-A.

Although G-comp is widely used for position control of manipulators [27], its importance in force interaction has not been well discussed. Realization of G-comp in multi-DoF humanoid robots considering multiple contact points and balancing is not straightforward; no solution has yet been reported. The optimal contact force distribution described in the subsequent section enables us to apply G-comp to various humanoid and mobile robots with various contact situations (e.g., bipedal or quadrupedal, single or double support phase).

C. Optimal Load Distribution to Multiple Contact Points

The GAF controller derived in (12) is insufficient for humanoid robots interacting with the environment at multiple contact points. However, it is not easy to solve for the required joint torques because of multiple kinematic loops [24]. For example, if the robot is in the double support phase or quadruped phase, there are many possible combinations of the commanded joint torques that result in the same desired GAF. Our solution is to compute the force closure first explicitly, then transform them to the joint torques using a passivity-based framework, as in the previous section. Therefore, the problem in this section is how to distribute the desired GAF to multiple contact points. To treat force control in a task space in a simple but uniform manner, we first solely consider the translational forces of the active force application points. We do not ignore moment and orientation: they can be controlled by combining multiple translational forces, as demonstrated in Section III-C.

Fig. 4 illustrates some contact situations with the force application points, together with the GAF and *CoP*. All of the related position vectors run from the CoM. Assuming that we are interested in a total of α contact points defined as $r_S = [r_{S1},\ r_{S2}, \ldots, r_{S\alpha}]^T \in \mathcal{R}^{3\alpha}$, where each vector component is $r_{Si} = [x_{Si},\ y_{Si},\ z_{Si}]^T \in \mathcal{R}^3$ for each index i, the associated applied contact forces are defined as $f_S = [f_{S1},\ f_{S2}, \ldots, f_{S\alpha}]^T \in \mathcal{R}^{3\alpha}$, where each vector component is $f_{Si} = [x_{Si},\ y_{Si},\ z_{Si}]^T \in \mathcal{R}^3$. In this description, f_S is the force that the robot applies to the contact points (care is needed in the force direction). Of course, CoP r_P must lie within the supporting convex hull of r_{Sj}. We are also interested in the total of β nonground contact points or interaction points as $r_F = [r_{F1},\ r_{F2}, \ldots, r_{F\beta}]^T \in \mathcal{R}^{3\beta}$ and their associated applied forces $f_F = [f_{F1},\ f_{F2}, \ldots, f_{F\beta}]^T \in \mathcal{R}^{3\beta}$. For example, $\alpha = 8$ and $\beta = 8$ in Fig. 4(a), but $\alpha = 4$ and $\beta = 12$ in Fig. 4(b). The discussion here is independent from robot models, and the number and the location of the contact points are arbitrary; they are applicable to one-legged, bipedal, and quadrupedal robots, as long as CoP is definable. It should be noted that the contact points do not necessarily lie in the same plane, as shown in Fig. 4.

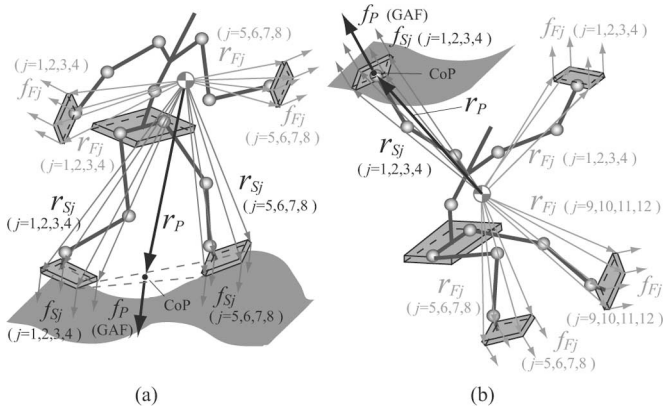

Fig. 4. Definition of GAF, contact points, and forces: each ground contact point r_{Sj} is assigned the contact force f_{Sj}, and each nonground contact point r_{Fj} is assigned with the interaction force f_{Fj}. The contact forces f_{Sj} are determined using a desired GAF f_P and f_{Fj}. The CoP r_P always lies within the supporting convex hull of r_{Sj}. (a) Unilateral contact (supported). (b) Bilateral contact (hung).

Our strategy is distributing the GAF to each ground contact point *through* CoP. From the definition, CoP can be expressed as

$$x_P = \frac{\sum_{j=1}^{\alpha} x_{Sj} f_{zSj}}{\sum_{j=1}^{\alpha} f_{zSj}}, \qquad y_P = \frac{\sum_{j=1}^{\alpha} y_{Sj} f_{zSj}}{\sum_{j=1}^{\alpha} f_{zSj}} \quad (19)$$

while the GAF is the sum of the respective contact forces:

$$f_P = \sum_{j=1}^{\alpha} f_{Sj}. \quad (20)$$

In simple notation, these two equations combine to

$$\begin{bmatrix} x_P \\ y_P \\ 1 \end{bmatrix} f_{zP} = \underbrace{\begin{bmatrix} x_{S1} & x_{S2} & \cdots & x_{S\alpha} \\ y_{S1} & y_{S2} & \cdots & y_{S\alpha} \\ 1 & 1 & \cdots & 1 \end{bmatrix}}_{A_z \in \mathcal{R}^{3\times\alpha}} \begin{bmatrix} f_{zS1} \\ f_{zS2} \\ \cdots \\ f_{zS\alpha} \end{bmatrix} \quad (21)$$

where A_z represents a *contact-force distribution matrix*.

Given a desired normal GAF $\bar{f}_{zP}$ and CoP $\bar{r}_P$ (see Section III-A for the balancing control case), we can calculate the corresponding desired normal contact forces $\bar{f}_{zS}$. Specifically, we

propose an optimal contact force distribution calculated as

$$\begin{bmatrix} \bar{f}_{zS1} \\ \bar{f}_{zS2} \\ \cdots \\ \bar{f}_{zS\alpha} \end{bmatrix} = A_z^{\#} \begin{bmatrix} \bar{x}_P \\ \bar{y}_P \\ 1 \end{bmatrix} \bar{f}_{zP} \tag{22}$$

with $A_z^{\#} = A_z^T (A_z A_z^T)^{-1}$. This solution is optimal in the sense that it minimizes the L_2 norm of the total contact forces. Because of the convexity of the contact points, the resultant normal contact force $\bar{f}_{zS}$ cannot be positive (therefore, the unilateral constraint condition is met) as long as $\bar{f}_{zP}$ is negative definite and the desired CoP $\bar{r}_P$ is set within the supporting convex hull (they are obvious restrictions).[2]

Similarly, we use

$$\begin{bmatrix} x_P \\ 1 \end{bmatrix} f_{xP} = \underbrace{\begin{bmatrix} x_{S1} & x_{S2} & \cdots & x_{S\alpha} \\ 1 & 1 & \cdots & 1 \end{bmatrix}}_{A_x \in \mathcal{R}^{2\times\alpha}} \begin{bmatrix} f_{xS1} \\ f_{xS2} \\ \cdots \\ f_{xS\alpha} \end{bmatrix} \tag{23}$$

$$\begin{bmatrix} y_P \\ 1 \end{bmatrix} f_{yP} = \underbrace{\begin{bmatrix} y_{S1} & y_{S2} & \cdots & y_{S\alpha} \\ 1 & 1 & \cdots & 1 \end{bmatrix}}_{A_y \in \mathcal{R}^{2\times\alpha}} \begin{bmatrix} f_{yS1} \\ f_{yS2} \\ \cdots \\ f_{yS\alpha} \end{bmatrix} \tag{24}$$

to distribute the horizontal contact forces *in proportion to* the normal contact forces

$$\begin{bmatrix} \bar{f}_{xS1} \\ \bar{f}_{xS2} \\ \cdots \\ \bar{f}_{xS\alpha} \end{bmatrix} = A_x^{\#} \begin{bmatrix} \bar{x}_P \\ 1 \end{bmatrix} \bar{f}_{xP} \tag{25}$$

$$\begin{bmatrix} \bar{f}_{yS1} \\ \bar{f}_{yS2} \\ \cdots \\ \bar{f}_{yS\alpha} \end{bmatrix} = A_y^{\#} \begin{bmatrix} \bar{y}_P \\ 1 \end{bmatrix} \bar{f}_{yP} \tag{26}$$

so that the contact points with larger normal contact force receive more ground friction.

As a consequence, a desired GAF might be distributed over the desired contact forces using a simple matrix operation

$$\bar{f}_S = A^{\#} \begin{bmatrix} \bar{x}_P \bar{f}_{xP} \\ \bar{f}_{xP} \\ \hline \bar{y}_P \bar{f}_{yP} \\ \bar{f}_{yP} \\ \hline \bar{x}_P \bar{f}_{zP} \\ \bar{y}_P \bar{f}_{zP} \\ \bar{f}_{zP} \end{bmatrix} \tag{27}$$

where in $A = \mathrm{diag}(A_x, A_y, A_z)$ is the total contact force distribution matrix.

[2]As a trivial extension, we can introduce a weight into the optimal criteria as $\bar{f}_{zS}^T W \bar{f}_{zS}$, where $W \in \mathcal{R}^{\alpha\times\alpha}$ is the weighting matrix. The optimal force closure is given as (22), but with $A_z^{\#} = W^{-1} A_z^T (A_z W^{-1} A_z^T)^{-1}$. The weighting might be useful when we need to consider the friction cone of the ground explicitly, or when we need to reduce the load to some limbs because of breakage of some joints.

D. Summary

Finally, the commanded joint torques are obtainable as

$$\tau = J_S(q)^T \bar{f}_S + \zeta(q, \dot{q}) \tag{28}$$

where $J_S(q) \in \mathcal{R}^{3\alpha\times n}$ represents the contact Jacobian from the CoM to the supporting contact points (derivative of r_S with respect to q), where G-comp $\bar{f}_P = f_v + Mg$ must be included in the calculation of $\bar{f}_S$.

The overall control procedure can be summarized as follows.

P1) Calculate all forward kinematics.
P2) Set the user task force f_u for given task objectives.
P3) Calculate the desired GAF $\bar{f}_P$ by $\bar{f}_P = f_u + Mg$.
P4) Determine the contact points r_{Sj} $(j \in \{1, 2, \ldots, \alpha\})$ and active joints q_i $(i \in \{1, 2, \ldots, n\})$; then remove row and column vectors according to inactive joints or contacts.
P5) Calculate the desired contact forces $\bar{f}_S$ by (27).
P6) Transform the contact forces $\bar{f}_S$ to torque commands τ for the active joints by (28).

Some notes are in order.

1) The attitude of the base, obtained by using the gyro sensor, is also included in q; hence, in the Jacobians.
2) The proposed method requires no contact force measurement, but it does require kinematic information of the supporting contact points, which are *preset* by the user.
3) The contact forces are computed according to the current shape of the supporting convex hull, where respective preset contact points do not necessarily lie on the same plane.
4) The gound contact points should be defined so that the convex hull includes the *actual* CoP in it.
5) Even if some contact point loses its contact with the ground, the controller still *assumes* that its contacts are active. It, therefore, distributes the contact forces to all the preset contact points.
6) We can remove the *row* vector from $J_S(q)$ if some contact point loses contact with the environment (requires tactile information). However, this is not always a good solution.
7) Similarly, if some joints are specified with trajectories or hit the range of motion, we can simply remove the corresponding *column* vector from $J_S(q)$.
8) We do not consider that defective case in which the task space control objects are too numerous compared to the number of joints. Clearly, we cannot achieve the tasks simultaneously in this case.
9) The control torques generated by (28) differ from those of (12) because it uses the null space of J_P by specifying the contact forces.
10) The means to achieve the desired joint torques depends on the hardware (see Section IV-A).

At this point, we have not discussed the balancing tasks or force interaction tasks. We have merely described convergence of the GRF and internal motions under gravity compensation control. That is, we have not yet discussed how to give the user task force f_u [(P2) in the aforementioned procedure]. These issues are described in the next section.

III. Force Interaction Control With Balance

This section explains simple controllers for force interaction with balancing based on linear feedback. Section III-A shows a simple CoP-constrained balancer. Section III-B shows a simple method for controlling the position and force of hands or swinging legs for force-interaction tasks. Section III-C describes how to generate rotational moments and achieve desired orientations of the base, hands, etc., and how to compensate yaw moment.

A. Balance Control

The balance control discussed in this section is asymptotic stabilization of the ground projection of CoM to some target position in the supporting convex hull. A simple feedback law can be used

$$f_u = -K_{PC}(r_C - \bar{r}_C) - K_{DC}(\dot{r}_C - \dot{\bar{r}}_C) \tag{29}$$

with some desired CoM position/velocity $\bar{r}_C,\ \dot{\bar{r}}_C$, and the task-space potential difference (PD) gains $K_{PC}, K_{DC} > 0$. Of course, we can incorporate feed-forward term $M\ddot{\bar{r}}_C$ in it. A lower bound is set for $\bar{f}_{uz}$ to prevent the robot from losing all contact with the ground.

Recall that CoP is, by definition, the representative force application point because it is the weighted sum of the translational ground contact forces as in (20). On the other hand, the *zero moment point} (ZMP*) is defined as a point on the ground at which total moments balance (see [29] and references therein), which is denoted as $r'_P = [x'_P,\ y'_P,\ z_P]$. Since we do not want to calculate a complex nonlinear term, we use a "simple version" of ZMP. Specifically, we assume that the rate change of the angular momentum around CoM is negligible. In this case, ZMP can be written as follows:

$$x'_P = \frac{z_P m\ddot{x}_C}{m(\ddot{z}_C + g)} = \frac{z_P f_{xP}}{f_{zP}}$$
$$y'_P = \frac{z_P m\ddot{y}_C}{m(\ddot{y}_C + g)} = \frac{z_P f_{yP}}{f_{zP}}. \tag{30}$$

Therefore, with our G-comp strategy (11) and user force input (29), the desired ZMP $\bar{r}'_P$ is set to

$$\bar{x}'_P = \frac{z_P f_{ux}}{mg + f_{uz}}, \qquad \bar{y}'_P = \frac{z_P f_{uy}}{mg + f_{uz}}. \tag{31}$$

In these equations, $z_P = -z_C$. It should be noted that this ZMP can exit from the supporting region depending on the desired GAF. We restrict ZMP into the supporting convex hull to incorporate the balancing controller with our contact force distribution about CoP (27). We can modify the horizontal GAF (f_{ux} and f_{uy}) and/or normal GAF (f_{uz}) to achieve this. In this case, the modified ZMP coincides with CoP because the moment balances at CoP. We use this as the desired CoP for balancing.[3] That is, we set

$$\bar{r}_P = \bar{r}'_P. \tag{32}$$

Finally, the modified GAF $\bar{f}_P$, in addition to the desired CoP $\bar{r}_P$, are then used for determining the desired contact force closure in (P5) in Section II-D. We call this restricted but simple balance controller a "CoP-constrained balancer."

The balancing performance is demonstrated in Section IV.

An intuitive interpretation is available by considering a special case: $\bar{f}_{xP} = \bar{f}_{yP} = 0$ (G-comp only). In this case, the desired ZMP (or CoP) coincides with the ground projection of CoM, $\bar{x}_P = \bar{y}_P = 0$, *if* they are inside the supporting region. Since the gravity is compensated, the CoM exhibits constant velocity movement.

B. Reaching-and-Force Interaction Tasks

Using our contact force framework, the motion command for supporting leg joints or swinging leg joints can be handled in a uniform manner. Contact forces at the interested contact points are used for task space force control, and also for position tracking. For example, we can use the interaction forces f_{Fj} for controlling the position r_{Fj} of the swinging legs or hands using a simple PD feedback law

$$\bar{f}_{Fj} = -K_{PF}(r^W_{Fj} - \bar{r}^W_{Fj}) - K_{DF}(\dot{r}^W_{Fj} - \dot{\bar{r}}^W_{Fj}),$$
$$j = 1, 2, \ldots, \beta \tag{33}$$

for given desired positions and velocities $\bar{r}^W_{Fj} = r_C + \bar{r}_{Fj}$, $\dot{\bar{r}}^W_{Fj} = \dot{r}_C + \dot{\bar{r}}_{Fj}$ in the world coordinate frame and positive gain matrices $K_P, K_D > 0$, or by a feed-forward force command. The control torque is simply given as

$$\tau_f = J_F(q)^T \bar{f}_F \tag{34}$$

where $J_F(q) = \partial r_F / \partial q$ is the task Jacobian.

Even if the task control force is zero $\bar{f}_F = 0$, the swinging legs or hands are gravity-compensated and the internal motions are damped by the main full-body force controller (28). However, we must deactivate the contribution from balancing force input f_u to those joints wherein $J_F(q)$ is involved if we require that the reaching and force interaction task have the same priority as the balancing control. In this case, we can hold the swinging legs or hands and move them with a slight external force applied to arbitrary contact points.

To achieve good tracking of a desired GAF $\bar{f}_P$, the interaction forces must be compensated.[4] This can be accomplished by simply subtracting the sum of the interaction forces from the desired GAF *in advance*:

$$\bar{f}_P \xleftarrow{\text{substitute}} \bar{f}_P - \sum_{j=1}^{\beta} \bar{f}_{Fj}. \tag{35}$$

However, this is an approximated compensation. Perfect compensation requires precise forward dynamics (moments of inertia identification and velocity measurement).

[3] By limiting ZMP into the supporting region, the desired GAF might become small, which might restrict the balancing ability. We should not restrict ZMP if we want to enhance the balancing ability. However, we must revert to full nonlinear dynamics [inverse of (7)] to achieve the desired ZMP. See [22] for example. A simple controller that does not necessitate solving full nonlinear dynamics is under development.

[4] If CoM state feedback such as (29) is employed and the motions of legs/hands are sufficiently slow, the force/moment compensation is not necessary.

C. Moment Generation by Contact Forces

To this point, we have addressed the translational force GAF f_P. However, generation of moment is also crucial for full-body balancing. Our contact force framework is also applicable to the moment generation. As an illustration in this section, we will describe yaw moment control, which is very important for fast bipedal locomotion. Let T_z be the applied yaw moment around CoP. It is related to the contact forces by

$$T_z = \sum_{j=1}^{\alpha} \begin{bmatrix} x_{Sj} \\ y_{Sj} \end{bmatrix} \times \begin{bmatrix} f'_{xSj} \\ f'_{ySj} \end{bmatrix} \in \mathcal{R}^1 \tag{36}$$

or, in a simple form,

$$T_z = \underbrace{[-y_{S1}, \ldots, -y_{S\alpha}, x_{S1}, \ldots, x_{S\alpha}]}_{B \in \mathcal{R}^{1\times 2\alpha}} \begin{bmatrix} f'_{xS1} \\ \cdots \\ f'_{xS1} \\ f'_{ySa} \\ \cdots \\ f'_{ySa} \end{bmatrix} \tag{37}$$

where B represents a *contact-moment distribution matrix*. If we calculate the corresponding contact forces by inverting (37) for a desired yaw moment $\bar{T}_z$, the results, however, might contradict the previous contact forces (25) and (26). Therefore, we combine (23), (38), and (37) to

$$\begin{bmatrix} x_P f_{xP} \\ \hline f_{xP} \\ \hline y_P f_{yP} \\ \hline f_{yP} \\ \hline T_z \end{bmatrix} = \underbrace{\begin{bmatrix} A_x \\ A_y \\ B \end{bmatrix}}_{C} \begin{bmatrix} f_{xS1} \\ \cdots \\ f_{xS\alpha} \\ \hline f_{yS1} \\ \cdots \\ f_{yS\alpha} \end{bmatrix} \tag{38}$$

and invert it to obtain

$$\begin{bmatrix} \bar{f}_{xS1} \\ \cdots \\ \bar{f}_{xS\alpha} \\ \hline \bar{f}_{yS1} \\ \cdots \\ \bar{f}_{yS\alpha} \end{bmatrix} = C^{\#} \begin{bmatrix} \bar{x}_P \bar{f}_{xP} \\ \hline \bar{f}_{xP} \\ \hline \bar{y}_P \bar{f}_{yP} \\ \hline \bar{f}_{yP} \\ \hline \bar{T}_z \end{bmatrix}. \tag{39}$$

This paper proposes two important moment controllers. The first one is for controlling the base heading

$$\bar{T}_{z1} = -K_{PY}(e_3 - \bar{e}_3) - K_{DY}\dot{e}_3 \tag{40}$$

where $K_{PY}, K_{DY} > 0$ are gains and e_3 is the yaw orientation of the base. The second one is for compensating the yaw moment caused by a swinging leg's (or trunk's or hand's) motion:

$$\bar{T}_{z2} = -\sum_{j=1}^{\beta} \begin{bmatrix} (x_{Fj} - x_P) \\ (y_{Fj} - y_P) \end{bmatrix} \times \begin{bmatrix} \bar{f}_{xFj} \\ \bar{f}_{yFj} \end{bmatrix}. \tag{41}$$

The total target moment $\bar{T}_z = \bar{T}_{z1} + \bar{T}_{z2}$ is then substituted into the right-hand side (RHS) of (39) to obtain the desired horizontal contact forces.

Furthermore, orientation control for swinging legs or hands can be implemented similarly to (33); their motions are compensated easily by modifying the original contact forces. Specifically, we subtract the contact forces $\bar{f}'_{Sj}$ caused by the orientation control from the original contact forces, as in (35). That is,

$$\bar{f}_S \xleftarrow{\text{substitute}} \bar{f}_S + \sum_{j=1}^{\alpha} \bar{f}'_{Sj}. \tag{42}$$

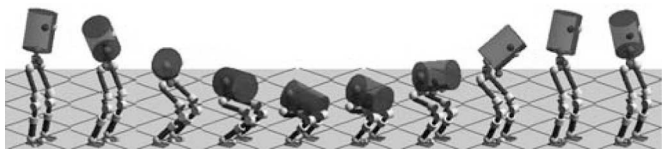

Fig. 5. Animation of a balanced squat with the torso swinging for 1–3 s: the desired CoM height and the torso orientation are simply given by sinusoidal trajectories, but no compensation (42) has been applied.

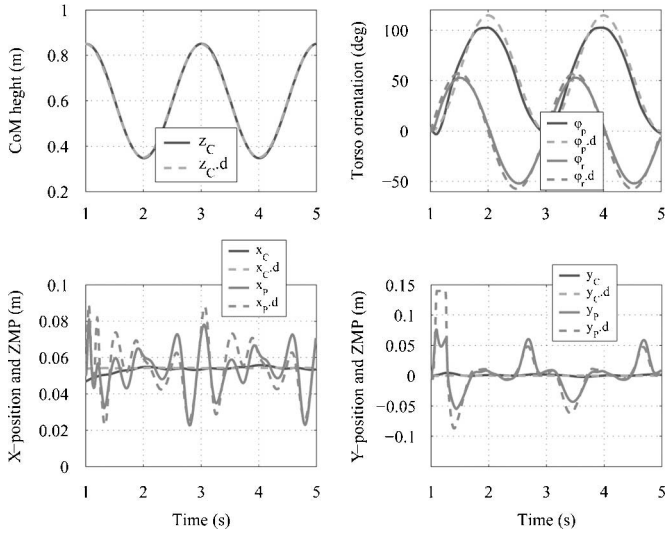

Fig. 6. Time evolution of the balanced squat in Fig. 5 : CoM (x_C, y_C, z_C) and ZMP (x_P, y_P) are shown along with their desired values (indicated by ".d").

D. Simulations of Balancing

Simulation results of balanced squatting with the torso orientation controlled are shown in Figs. 5 and 6. The simulator is built on a dynamics simulator SD/FAST (www.sdfast.com), where the ground contact is modeled as unilateral virtual springs and dampers. The desired CoP is allowed to travel from -0.05 m to $+0.1$ m in the X-direction when both feet are aligned.

The desired horizontal position of CoM is the center of the supporting convex hull, which is not fixed in Σ_W. The desired CoM height $\bar{z}_C$ and the torso orientation are given simply by sinusoidal trajectories, as shown in Fig. 6 . The gains described in (29) are set to $(K_{PC}, K_{DC}) = (5000, 500)$ for vertical motion and $(K_{PC}, K_{DC}) = (100, 50)$ for horizontal motion. The joint-wise damping in (15) was set as $D = \mathrm{diag}[d_1, d_2, \ldots, d_n]$ with $d_{\mathrm{legs}} = 2$ and $d_{\mathrm{torso}} = 8$.

A reaching task with balance is shown in Fig. 7. The CoM height z_C is not controlled, but is largely damped by the derivative gain K_{DC} in (29). Other parameters are identical to those

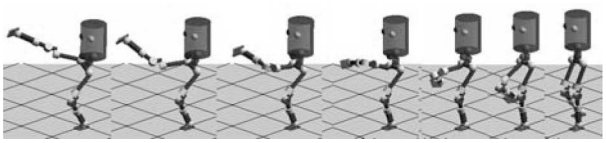

Fig. 7. Animation of a periodic reaching task by a leg with simultaneous balancing.

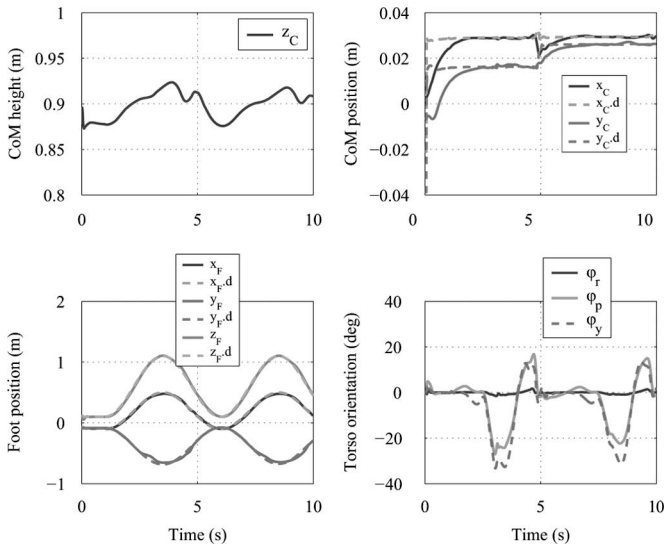

Fig. 8. Simulation result of a reaching task by a leg: the target foot positions indicated by $x_F.d, y_F.d, z_F.d$ are given by 0.2 Hz sinusoidal functions. The horizontal position of CoM x_C, y_C is regulated to the center of the foot.

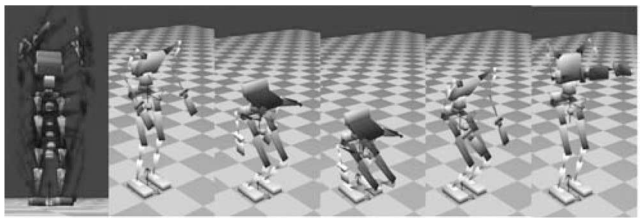

Fig. 9. Squatting on a full-body humanoid simulator.

given previously. The position of the swinging leg in Σ_W, r_F^W, is given as a sinusoidal function, as shown in Fig. 8. During the motion, the target equilibrium point, that is, the center of the supporting foot, is moved slightly because of the slip. Nevertheless, the horizontal CoM position x_C, y_C is stabilized to the *new* equilibrium (the center of the sole). In both simulations, small tracking errors in CoM are apparent. The errors originate in the uncompensated dynamics and persist as long as the robot is in motion.

Fig. 9 shows squatting in our new simulation environment, where the ground contact is modeled in an advanced manner [30]. The contact forces are distributed over the whole body, including the arms (the arm joints are moving).

IV. Experiments on Force Interaction

This section presents some experiments using the proposed method and our new humanoid robot prototype (Fig. 2). First, we briefly describe the robot hardware in Section IV-B. Then, we show the results of balancing with unknown external forces in Section IV-B, upper body interaction in Section IV-C, and interaction at different contact points on the lower body in Section IV-D. The robot is supported neither by hydraulic hoses nor by cables. They apply nonnegligible disturbances to the robot. All experiments in this paper are performed in the double support phase with an aligned feet configuration. However, the method is applicable to arbitrary shapes of a supporting convex hull without any modification.

A. Humanoid Platform and Joint Torque Control

The humanoid platform shown in Fig. 2(a) was developed by SARCOS and ATR [4], [5]. The robot is called computational brain (CB). The hip height is 0.82 m in an upright posture. The robot is attached with the cubic sole that is 0.12 m wide, 0.27 m long, and 0.02 m deep. Currently, the total weight is 93.7 kg. The DoF configuration is shown in Fig. 2(b). The arms and legs have 7 DoFs: there are 3 DoFs on the neck; the torso has 3 DoFs. There are 50 DoFs including the fingers (12 DoFs) and the eye cameras (4 DoFs). Most of the DoFs are driven by hydraulic servo actuators. Currently, all are operated by 21 MPa supply pressure. The robot is installed with position sensors and force sensors at each joint. A three-axis gyro sensor is attached to the base link. The actuators are controlled by small local controllers that provide low-level position, velocity, and force feedback loop. They are interconnected by a high-speed intranetwork [5]. The joint torque control is based solely on the force feedback of the force sensors attached to each joint. See [31] for the force control using hydraulic servo actuators and force sensors. The local controllers compute the feedback signal every 5 kHz and control the current into hydraulic servo valve using analog circuitry.

However, no joints are collocated with their actuators because the joints are driven by linear hydraulic actuators via linkage mechanisms. Moreover, most joints are not collocated with the force sensors. We, therefore, implemented local joint torque controllers based on the individual joint kinematics as follows.

i) Convert desired joint torques to the desired actuator forces.
ii) Calculate the reaction forces applied to the force sensors.
iii) Convert (L2) to the actuator reaction forces.
iv) Tracking (L3) to (L1) by high-speed local feedback control.

Kinematics of respective joints are represented using one-to-one trigonometric functions bounded by the range of motion. The trigonometric functions are approximated by up to third-order polynomials. The transformations described before are also applied to the joint angle controller. That is, the feedback computations are always done in the actuator space. Thereby, we ensure a *flat* actuator response irrespective of the joint configuration. Once the local joint torque control is established, it is straightforward to implement the controller. The control procedure (Section II-D) is simple. Moreover, it can be executed with a low computational cost. All the control processes are complete within 1 ms.

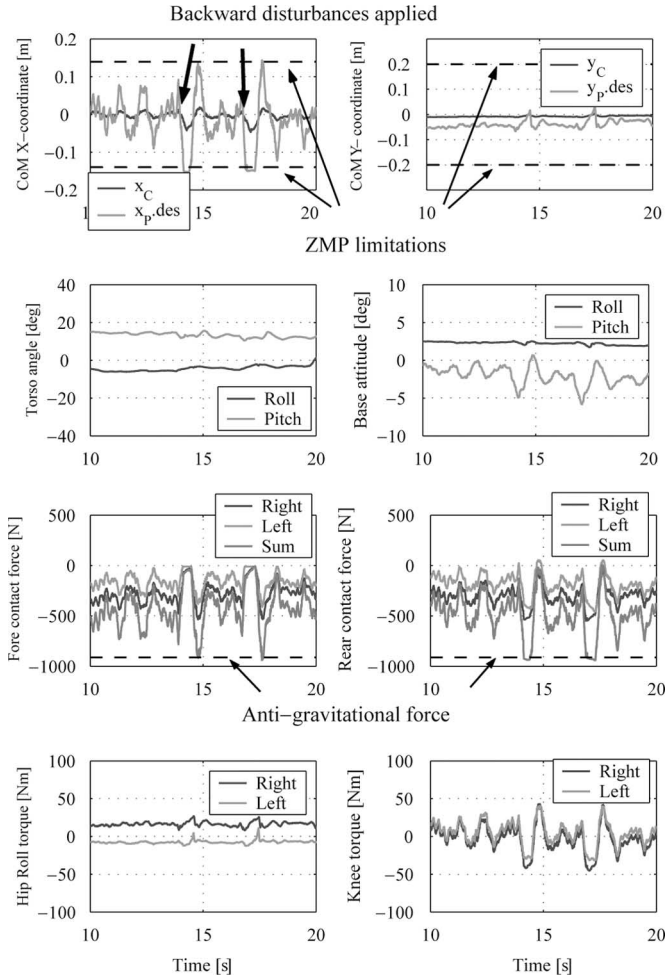

Fig. 10. Experimental data of balancing under disturbances: the disturbances are applied backwards twice. The third row shows the desired normal contact forces.

The supplementary video no. 1 shows an experimental result of gravity compensation for the lower body. The legs move as if there is no gravity if no interaction forces exist. This experiment demonstrates not only force interaction without balancing, but also the performance of the joint torque control.

B. Balancing Ability

An experimental result of balancing is shown in Fig. 10 (see also the supplementary video no. 2). Large disturbances were applied to the robot. The top two graphs show positions of the CoM and desired CoP. The limits on the desired CoP are indicated by two dashed lines, ± 0.135 m. The desired CoP always leads the CoM, which reflects that the controller applies a GAF so that the CoM converges to the desired position (zero in this example). The graphs in the third row depict the desired normal contact forces $\bar{f}_{zSj}$, as calculated using (22). The left graph shows the forces applied to the *fore* corners (right sole, $f_{zS1} + f_{zS2}$; left sole, $f_{zS5} + f_{zS6}$, and the sum); the right graph shows the contact forces applied to the *rear* corners (right sole, $f_{zS3} + f_{zS4}$; left sole, $f_{zS7} + f_{zS8}$, and sum). The indexes of the contact points are shown in Fig. 4(a). The dashed line indicates the total antigravitational force: $-mg$. The CoM height is not controlled in this example. Therefore, $\sum_{j=1}^{8} f_{zSj} = -mg$ holds. The graphs show that the antigravitational force is actually distributed over the normal contact forces appropriately by (22).

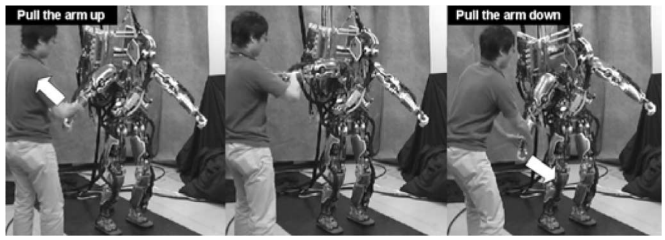

Fig. 11. Experiments on the upper-body interaction with balance. The human shakes the arm. Note that the GAF including the antigravitational force is distributed not only to the legs and the torso, but also to the arms. The robot is responding to the external force by the full-body compensatory motion.

A practical issue for model-based balance control is the definition of the origin of Σ_W. We propose a simple solution: defining the origin as the center point between the feet, which means that the origin is always moving according to the current robot configuration. Gyro information is important for both the CoM measurement and the desired GAF direction.

C. Upper Body Interaction

Experimental results for upper body interaction with balancing are shown in Fig. 11 (see also the supplementary video no. 4). The arms are shaken manually by the operator. In this experiment, the desired ground contact forces are also distributed to the arm joints.

In the experiment, the controller does not know how much external force is applied. However, if the controller knew the external forces *a priori*, it would be able to compensate them in an *anticipatory* manner by simply subtracting the forces to be compensated from the desired GAF in the same way as (35), which provides markedly better performance. For rich humanoid interaction, it will be desirable for the robot to have the ability to predict the partner's action based on observations including external forces, as indicated in Fig. 1.

D. Force Interaction at Different Contact Points on Lower Body

The location to apply the external force is arbitrary. Fig. 12 (see the supplementary video no. 3) shows the typical performance of our balancing controller when a side force is applied. This result nicely illustrates the relationship between the CoM error and the GRF distribution. In this example, CoM is largely laterally perturbed from the desired equilibrium (zero). The desired CoP is moved onto one edge of the foot while the desired CoM is fixed to the center. When this happens, the desired normal contact forces of the other foot become nearly zero. For that reason, one foot loses its contact with the ground and lifts off. In this example, however, we applied no position control for swinging leg. Therefore, the lifted foot moves purely as a result of the balancing control.[5] In this case, the

[5]In [32], we presented an active stepping control for disturbance rejection against huge external force.

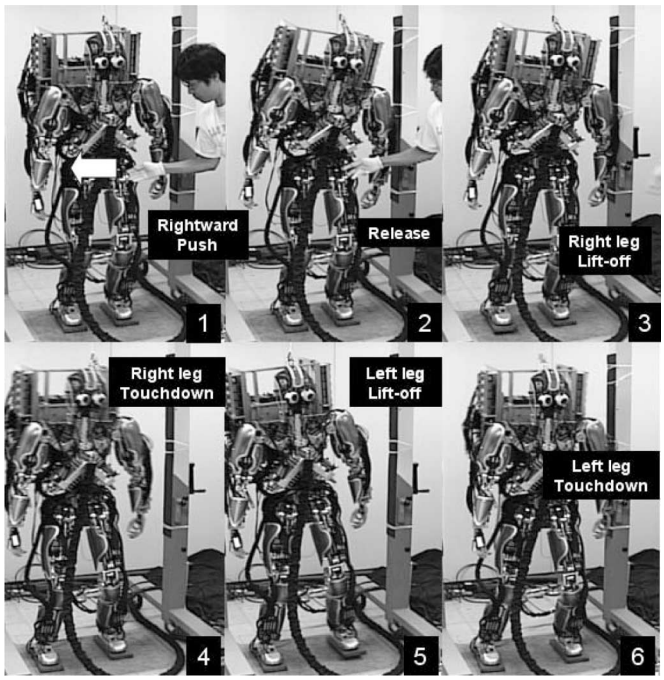

Fig. 12. Our force distribution law reduces some contact forces when a large error in CoM is detected. As a result, a foot might lift off of the ground.

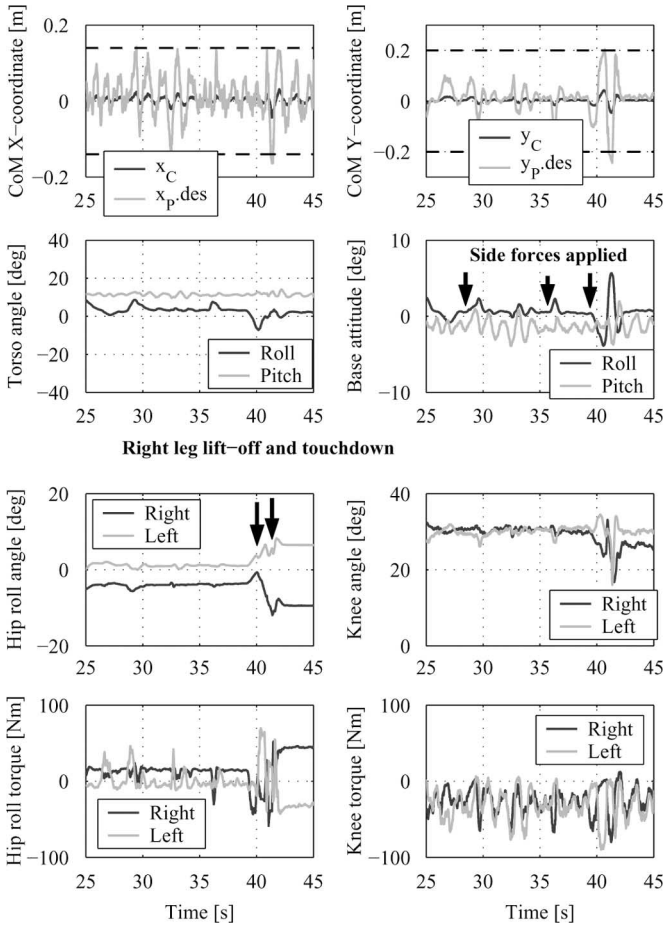

Fig. 13. Experimental data corresponding to Fig. 12.

foot moves to the outside. Simultaneously, the CoM moves back to the center of the feet. Then, the lifted foot touches the ground. This process executes once more; finally, the robot balances, but with a different configuration from the initial one. Fig. 13 shows the time evolution of this experiment. The top two graphs show the positions of CoM and the desired CoP. Of course, the lifted foot does not move if we apply some feedback controller to maintain the distance between each foot.

A salient point is that we do not specify which joints should move in compliance with the disturbances. For example, we use no weighting matrix, as in some inverse kinematics approach. The weighting is done automatically by the Jacobian *transpose* $J_S(q)^T$ in (28), and the compensating contact forces are distributed to the joint torques of the *whole* body. Therefore, if we push the robot torso, the torso compliantly follows first; then the lower body begins to compensate for the CoM error. Similarly, if we push the hip, the hip moves first, as shown in Figs. 14 and 15. We can even apply external forces to the leg joints. For example, if we push the knee, the knee joint follows compliantly to the external force; then the remaining joints generate compensatory torques to retain the balance. This can be seen from Fig. 16 (and the supplementary video no. 4). Although the controller does not measure the external force, the response to the external force is *immediate*. The reason is that most joints are commanded to have *zero* torque when the robot has upright posture (equilibrium). The compliance is not only important for natural and safe human–humanoid interaction. It is also crucial to make the robot perform human-like behavior.

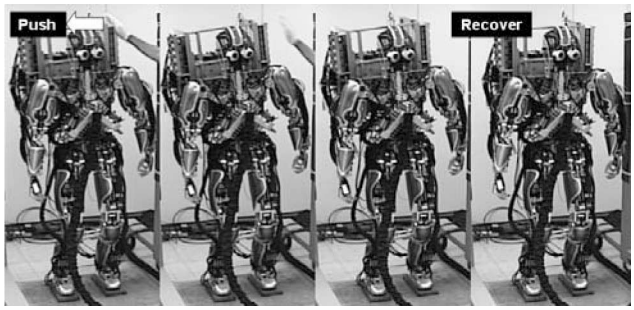

Fig. 14. Compensatory motion for a side push at the back.

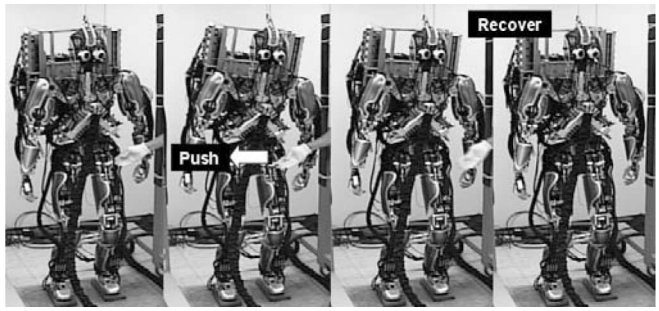

Fig. 15. Compensatory motion for a side push at the hip.

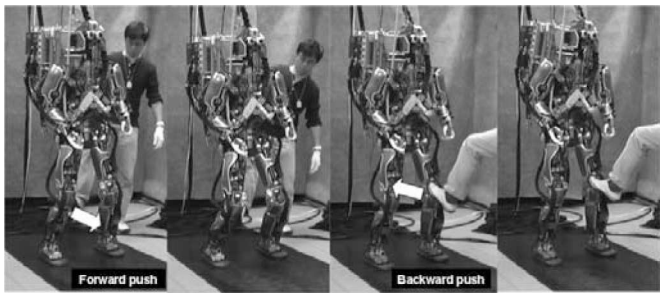

Fig. 16. Compensatory motions for a push at the knee.

V. Discussion

A. Comparison With Related Position-Based Balancers

We compare our method to some position-based controllers for humanoid robots, in which each joint is controlled by a position servo controller that requires joint angle command. To our knowledge, [12] is the first report of a biped robot demonstrating balance against large disturbances. Based on a simple linear inverted pendulum, this controller assumes ZMP fixed to some point and calculates the necessary compensatory joint motions in real time, then applies a local position controller. One method [13] is based on a similar inverted pendulum model, but it allows ZMP to move according to the state of CoM. These methods also differ in the manner in which the disturbances or CoM states are measured: the former measures contact forces directly, whereas the latter measures the GRF. An additional difference is the weight assignment for the compensating DoF: the former uses trunk compensation; the latter uses waist compensation. Mixed weight assignment has also been proposed in [14]. This concept was extended to whole-body motion control in [16] and [33]. For example, in [33], the Jacobian inverse

$$\dot{q} = J_P(q)^{\#}(-\dot{\bar{r}}_P) \tag{43}$$

is employed for some desired CoM velocity $-\dot{\bar{r}}_P$. Herein, $J_P^{\#} = W^{-1}J_P^T(J_P W^{-1} J_P^T)^{-1}$ is the weighted pseudoinverse with the weighting matrix W, which should be specified in advance. This type of controller works well if the external forces are measured. Usually, these methods assume GRF measurement; the controller can compute the compensatory motions according to the desired GRF or CoM position.

However, if the external force is applied to some point at which the force sensor is not installed, we encounter a problem. For example, we assume that a disturbance is applied to the waist. The joints are position controlled. Therefore, the disturbance changes the CoM as well as the ZMP. The method [13] modifies the desired ZMP to recover the balance. Then, to achieve the actual ZMP track to the desired ZMP, the controller accelerates the waist position. That is, if we push the robot waist, the waist immediately counteracts the external force. This behavior is undesirable for humanoid interaction for safety reasons and differs from what a human does. Although the controller (43) can handle weight assignment, we cannot anticipate, *in principle*, which joint must move in compliance to the *unknown* external forces.

B. Comparison With Related Force-Based Controllers

By "force-based controllers," we mean those controllers that require commanded joint torques rather than the joint angle. In [34], a simple static force control is applied to a 2-D bipedal walking robot driven by a novel force-controllable actuator prototype. This work is the first result of force-based walking.

Although not implemented for real robots, the method [36] for fixed-base robotic manipulators was recently extended to full-body humanoid motion control in [35] with multilevel prioritization. This method is useful if we have multiple task objectives because it can handle task prioritization explicitly. That control strategy differs from ours because it accompanies the exact cancelation of nonlinear dynamics.

The most closely related work to this paper is [37]. They applied similar passivity-based controller to redundant flexible manipulator. The manipulator is fixed to the ground. Consequently, the balance issue is not addressed. However, they achieved excellent experimental results on gravity compensation and force interaction by their dual manipulator, which is driven by electric servo motors and harmonic gears and installed with torque sensors.

VI. Conclusion

In this paper, we presented our motivation for studying humanoid robots in terms of their suitability to anthropogenic environments, general adaptability, intuitive relationship with humans, and value as experimental tools informing and inspiring our ongoing investigation of ourselves as humans. We explained the importance of the physical interaction between humans and life-size humanoid robots, and described our integrated system paradigm for development of humanoid robot technology. In this context, we, therefore, clarified the need for a robust and general technique for maintaining balance in bipedal humanoid robots in the form of an integrated subsystem that might accommodate the requirements of high-level motion planning and interpretation.

The primary technical contribution of this paper is a full-body passivity-based force-level balancing control strategy incorporating gravity compensation, thereby effortlessly accommodating an arbitrary number of external force interaction points, and obviating force sensors at the contact points. Using a passivity-based strategy, contact forces are well controlled in a satisfactory dynamic range without computing awkward dynamic terms, whereas internal motions are well suppressed. The method identifies a desired applied force from the robot to the environment, such as antigravitational force, which is distributed optimally over the forces acting at arbitrary contact points, and which is then transformed directly into whole-body joint torques. We performed various balancing experiments on a real hardware platform under unknown external forces and demonstrated the effectiveness of the method. In particular, we confirmed the following benefits.

1) Measurement of contact forces is not necessary.
2) An arbitrary number of contact points can be handled at little or no additional computational cost.

3) Arbitrary shape of the supporting convex hull is applicable.
4) Solving inverse kinematic and inverse dynamic problems is not necessary, joint trajectories are not necessary, and whole control algorithms are executed in real time without any recursive computation.
5) Joint friction is used to suppress internal motion.
6) Whole-body compliant balancing is possible in the presence of unknown external forces applied to arbitrary joint segments.
7) Joint movements for interaction or reaching can be achieved easily using a naive superposition or approximate compensation.

Our future work will elaborate a model of physical interaction blending high-level motion planning with automatic balance control, as depicted in Fig. 1. Building on the reliable technique, we have developed for maintaining balance in a way that can be combined with arbitrary uses of the body while accomplishing tasks.

APPENDIX I
DERIVATION OF STATIC JOINT FORCE CONTROLLER

It is straightforward to prove that (8) and (9) yields (10) when $\gamma \approx 0$, $\hat{C} \approx 0$. By substituting (8)

$$\tau = J_P^T (f_v + Mg)$$

into

$$f_P \approx (\hat{E}\hat{I}^{-1}\hat{E}^T)^{-1}\{\hat{E}\hat{I}^{-1}(u - \hat{G})\} \tag{44}$$

and expanding the RHS, we obtain

$$\begin{aligned}
&\hat{E}\hat{I}^{-1}\hat{E}^T \\
&= [\, id \,|\quad J_P \,] \begin{bmatrix} M & 0 \\ 0 & I \end{bmatrix}^{-1} \begin{bmatrix} \frac{id}{Jp^T} \end{bmatrix} \\
&= M^{-1} + J_P I^{-1} J_P^T
\end{aligned} \tag{45}$$

and

$$\begin{aligned}
&\hat{E}\hat{I}^{-1}(u - \hat{G}) \\
&= \hat{E}\hat{I}^{-1} \left(\begin{bmatrix} 0 \\ \frac{}{Jp^T (Mg + f_v)} \end{bmatrix} + \begin{bmatrix} Mg \\ \frac{}{0} \end{bmatrix} \right) \\
&= \hat{E}\hat{I}^{-1}\hat{E}^T Mg + \hat{E}\hat{I}^{-1} \begin{bmatrix} 0 \\ \frac{}{Jp^T f_v} \end{bmatrix} \\
&= \hat{E}\hat{I}^{-1}\hat{E}^T Mg + \left(J_P I^{-1} J_P^T\right) f_v.
\end{aligned} \tag{46}$$

With reference to (45) and (46), (44) becomes

$$f_P \approx Mg + \left(M^{-1} + J_P I^{-1} J_P^T\right)^{-1} \left(J_P I^{-1} J_P^T\right) f_v. \tag{47}$$

If we give f_v as (9), that is,

$$\begin{aligned}
f_v &= (J_P I^{-1} J_P^T)^{-1}(M^{-1} + J_P I^{-1} J_P^T) f_u \\
&= f_u + (J_P I^{-1} J_P^T)^{-1} M^{-1} f_u
\end{aligned}$$

we recover (10):

$$f_P \approx f_u + Mg.$$

APPENDIX II
CONVERGENCE OF THE CONTACT FORCE

It is also straightforward to prove (12)

$$\tau = J_P^T (f_v + Mg) + \zeta(q, \dot{q})$$

achieves (13) when (14) is stable. For illustration, we substitute $\tau = J_P^T Mg + \zeta$ into (7):

$$f_P = (\hat{E}\hat{I}^{-1}\hat{E}^T)^{-1}\{\gamma + \hat{E}\hat{I}^{-1}(u - \hat{C} - \hat{G})\}.$$

The upper part of $\{\ \}$ becomes zero, whereas the lower part becomes

$$\gamma_2 + J_P I^{-1}(\zeta - C) =: w \tag{48}$$

where γ_2 is the lower half of $\gamma = [\gamma_1,\ \gamma_2]^T$. On the other hand, the lower part of (6)

$$\hat{E}(q)\ddot{\hat{q}}_C + \gamma(q, \dot{q}) = 0$$

can be written as

$$J_P \ddot{q} + \gamma_2 = 0. \tag{49}$$

Combining (48) and (49) yields

$$w = -J_P I^{-1}\{I\ddot{q} + C - \zeta\}. \tag{50}$$

Therefore, if we design ζ so that $I\ddot{q} + C - \zeta = 0$ is met (exact nonlinear compensation) or $I\ddot{q} + C - \zeta$ is asymptotically stable, that is, $\dot{q} \to 0$ as $t \to \infty$ (e.g., via damping injection), then $w \to 0$ as $t \to \infty$. Combining this with the result from Appendix I, we recover (13)

$$f_P \to f_u + Mg\ (t \to \infty).$$

ACKNOWLEDGMENT

The robot was developed for the National Institute of Communication Telecommunication (NiCT) in an NiCT–Advanced Telecommunications Research Institute International (ATR) collaboration. The authors would like to acknowledge the continued support of the members of SARCOS Research Corporation. They would also like to thank the anonymous reviewers for their helpful comments and suggestions.

REFERENCES

[1] C. Breazeal, *Designing Sociable Robots*. Cambridge, MA: MIT Press, 2002.
[2] H. Ishiguro and T. Minato, "Development of androids for studying on human–robot interaction," in *Proc. 36th Int. Symp. Robot.*, Boston, MA, Dec. 2005, p. TH3H1.
[3] E. Oztop, D. W. Franklin, T. Chaminade, and G. Cheng, "Human–humanoid interaction: Is a humanoid robot perceived as a human?," *Int. J. Humanoid Robot.*, vol. 2, no. 4, pp. 537–559, Dec. 2005.
[4] M. Kawato, ""Understanding the brain by creating the brain," towards manipulative neuroscience," *Philos. Trans. Roy. Soc.*, to be published.

[5] G. Cheng, S. Hyon, J. Morimoto, A. Ude, J. G. Hale, G. Colvin, W. Scroggin, and S. C. Jacobsen, "CB: A humanoid research platform for exploring neuroscience," *Adv. Robot.*, vol. 21, no. 10, pp. 1097–1114, 2007.
[6] Y. Kuniyoshi and A. Nagakubo, "Humanoid as a research vehicle into flexible complex interaction," in *Proc. IEEE/RSJ Int. Conf. Intell. Robots Syst.*, Grenoble, France, vol. 2, 1997, pp. 811–819.
[7] M. Asada, K. F. MacDorman, H. Ishiguro, and Y. Kuniyoshi, "Cognitive developmental robotics as a new paradigm for the design of humanoid robots," *Robot. Auton. Syst.*, vol. 37, pp. 185–193, 2001.
[8] R. Gregory, *Mind in Science*. Cambridge, U.K.: Cambridge Univ. Press, 1981.
[9] G. Cheng, A. Nagakubo, and Y. Kuniyoshi, "Continuous humanoid interaction: An integrated perspective—Gaining adaptivity, redundancy, flexibility—In one," *Robot. Auton. Syst.*, vol. 37, pp. 161–183, 2001.
[10] J. G. Hale and E. Pollick, "Sticky hands: Learning and generalization for coorporative physical interactions with a humanoid robot," *IEEE Trans. Syst., Man, Cybern. C, Appl. Rev.*, vol. 35, no. 4, pp. 512–521, Nov. 2005.
[11] I. Kato, "WABOT-2: Autonomous robot with dexterous finger—Arm coordination control in keyboard performance," in *Proc. IEEE Int. Conf. Robot. Autom.*, Raleigh, NC, vol. 4, 1987, pp. 90–97.
[12] A. Takanishi, T. Takeya, H. Karaki, and I. Kato, "A control method for dynamic biped walking under unknown external force," in *Proc. IEEE Int. Workshop Intell. Robots Syst.*, Tsuchiura, Japan, Jul. 1990, pp. 795–801.
[13] K. Hirai, M. Hirose, Y. Haikawa, and T. Takenaka, "The development of the Honda humanoid robot," in *Proc. IEEE Int. Conf. Robot. Autom.*, Leuven, Belgium, May1998, pp. 1321–1328.
[14] J. Yamaguchi, E. Soga, S. Inoue, and A. Takanishi, "Development of a bipedal humanoid robot-control method of whole body cooperative dynamic biped walking," in *Proc. IEEE Int. Conf. Robot. Autom.*, Detroit, MI, May 1999, pp. 368–374.
[15] K. Nagasaka, H. Inoue, and M. Inaba, "Dynamic walking pattern generation for a humanoid robot based on optimal gradient method," in *Proc. IEEE Int. Conf. Syst., Man, Cybern.*, Tokyo, Japan, Oct. 1999, vol. 6, pp. 908–913.
[16] S. Kajita, F. Kanehiro, K. Kaneko, K. Fujiwara, K. Harada, K. Yokoi, and H. Hirukawa, "Resolved momentum control: Humanoid motion planning based on the linear and angular momentum," in *Proc. IEEE/RSJ Int. Conf. Intell. Robots Syst.*, Las Vegas, NV, 2003, pp. 1644–1650.
[17] S. A. Setiawan, S. Hyon, J. Yamaguchi, and A. Takanishi, "Physical interaction between human and a bipedal humanoid robot-realization of human-follow walking," in *Proc. IEEE Int. Conf. Robot. Autom.*, Detroit, MI, May1999, pp. 361–367.
[18] S. Hyon and G. Cheng, "Passivity-based full-body force control for humanoids and application to dynamic balancing and locomotion," in *Proc. IEEE/RSJ Int. Conf. Intell. Robots Syst.*, Beijing, China, Oct. 2006, pp. 4915–4922.
[19] S. Hyon and G. Cheng, "Gravity compensation and full-body force interaction for humanoid robots," in *Proc. IEEE-RAS Int. Conf. Humanoid Robots*, Genova, Italy, Dec. 2006, pp. 214–221.
[20] D. T. Greenwood, *Classical Dynamics*. New York: Dover.
[21] L. Sciavicco and B. Siciliano, *Modeling and Control of Robot Manipulators*, 2nd ed. London, U.K.: Springer-Verlag, 1996.
[22] S. Hyon, N. Yokoyama, and T. Emura, "Back handspring of a multi-link gymnastic robot—Reference model approach," *Adv. Robot.*, vol. 20, no. 1, pp. 93–113, 2006.
[23] R. M. Murray, Z. Li, and S. S. Sastry, *A Mathematical Introduction to Robotic Manipulation*. Boca Raton, FL: CRC Press, 1994.
[24] R. Featherstone, *Robot Dynamics Algorithms*. Norwell, MA: Kluwer, 1987.
[25] S. Arimoto, M. Sekimoto, H. Hashiguchi, and R. Ozawa, "Natural resolution of ill-posedness of inverse kinematics for redundant robots: A challenge to Bernstein's degrees-of-freedom problem," *Adv. Robot.*, vol. 19, no. 4, pp. 401–434, 2005.
[26] S. Arimoto, M. Sekimoto, H. Hashiguchi, and R. Ozawa, "Physiologically inspired robot control: A challenge to Bernstein's degrees-of-freedom problem," in *Proc. IEEE Int. Conf. Robot. Autom.*, Barcelona, Spain, Apr. 2005, pp. 4500–4507.
[27] M. Takegaki and S. Arimoto, "A new feedback method for dynamic control of manipulators," *Trans. ASME J. Dyn. Syst., Meas. Control*, vol. 103, pp. 119–125, 1981.
[28] A. J. van der Schaft, *L2-Gain and Passivity Techniques in Nonlinear Control*. New York: Springer-Verlag, 1999.
[29] M. Vukobratović and B. Borovac, "Zero-moment point—Thirty five years of its life," *Int. J. Humanoid Robot.*, vol. 1, no. 1, pp. 157–173, 2004.
[30] J. G. Hale, "Contact handling with static and dynamic friction for dynamically simulated articulated figures," in *Proc. SCA 2006 Eurograph./ACM SIGGRAPH Symp. Comput. Animation*, Vienna, Austria, 2006, pp. 27–28.
[31] MOOG web site [Online]. Available: http://www. servovalve.com
[32] S. Hyon and G. Cheng, "Disturbance rejection for biped humanoids," in *Proc. IEEE Int. Conf. Robot. Autom.*, Rome, Italy, 2007, pp. 2668–2675.
[33] T. Sugihara and Y. Nakamura, "Whole-body cooperative balancing of humanoid robot using COG Jacobian," in *Proc. IEEE/RSJ Int. Conf. Intell. Robot. Syst.*, Lausanne, Switzerland, Sep. 2002, vol. 3, pp. 2575–2580.
[34] J. Pratt, C. Chew, A. Torres, P. Dilworth, and G. Pratt, "Virtual model control: An intuitive approach for bipedal locomotion," *Int. J. Robot. Res.*, vol. 20, no. 2, pp. 129–143, 2001.
[35] L. Sentis and O. Khatib, "Synthesis of whole-body behaviors through hierarchical control of behavioral primitives," *Int. J. Humanoid Robot.*, vol. 2, no. 4, pp. 505–518, 2005.
[36] O. Khatib, "A unified approach for motion and force control of robot manipulators: The operational space formulation," *IEEE J. Robot. Autom.*, vol. RA-3, no. 1, pp. 43–53, Feb. 1987.
[37] A. Albu-Schaffer, C. Ott, and G. Hirzinger, "A unified passivity-based control framework for position, torque and impedance control of flexible joint robots," *Int. J. Robot. Res.*, vol. 26, no. 1, pp. 23–39, 2007.

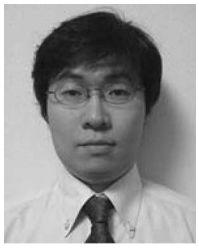

Sang-Ho Hyon (S'98–M'02) was born in Osaka, Japan. He received the M.Sc. degree in mechanical engineering from Waseda University, Tokyo, Japan, in 1998, and the Ph.D. degree in control engineering from Tokyo Institute of Technology, Tokyo, in 2002.

From 2002 to 2004, he was a Research Associate and Assistant Professor at the Graduate School of Engineering, Tohoku University, Japan. He is currently the Humanoid Dynamics and Locomotion Team Leader at the Computational Neuroscience Laboratories, Advanced Telecommunications Research Institute International (ATR), Kyoto, Japan, and a Researcher at the Japan Science and Technology Agency (JST), International Cooperative Research Project (ICORP), Computational Brain Project, Saitama, Japan. He has been engaged in developing many legged robots and the controllers, and in performing various dynamic locomotion experiments such as walking, running, jumping, and somersault. His current research interests include legged locomotion, humanoid robotics, dynamical systems, and nonlinear control theory.

Dr. Hyon received the 1999 International Conference on Robotics and Automation (ICRA) Best Paper Award Finalist. He is a member of the IEEE Robotics and Automation Society.

Joshua G. Hale was born in Lancaster, U.K. He received the B.A. and M.A. degrees in computation from the University of Oxford, Oxford, U.K., in 1997 and 2002, respectively, the M.Sc. degree in computer science from the University of Edinburgh, Edinburgh, U.K., in 1998, and the Ph.D. degree in biomimetic motion synthesis from the University of Glasgow, Glasgow, U.K., in 2003.

He was a Research Engineer at the Hardware Compilation Group, University of Oxford, and a Research Assistant at the Computer Vision and Graphics Laboratory, University of Glasgow. He is currently a Researcher at the Humanoid Robotics and Computational Neuroscience Laboratory, Advanced Telecommunications Research Institute International (ATR), Kyoto, Japan, and a researcher at Japan Science and Technology Agency (JST), International Cooperative Research Project (ICORP), Computational Brain Project, Saitama, Japan. His current research interests include computer graphics and 3-D modeling, human motion production and perception, dynamic simulation, and humanoid robotics.

Gordon Cheng (S'97–M'99–SM'06) received the Bachelor's and Master's degrees in computer science from the University of Wollongong, Wollongong, N.S.W., Australia, in 1991 and 1993, respectively, and the Ph.D. degree in systems engineering from the Department of Systems Engineering, Australian National University, Acton, A.C.T., Australia, in 1998.

He has held fellowships from the Center of Excellence (COE), Science, and Technology Agency (STA) of Japan at the Humanoid Interaction Laboratory, Intelligent Systems Division, ElectroTechnical Laboratory (ETL), Japan, where he developed a completely integrated humanoid robotics system. He has also been a consultant and a National Systems Manager for a major transport company. He was the Director of G.T.I. Computing, Australia, where he was engaged in networking/transport management systems. He is currently the Head of the Department of Humanoid Robotics and Computational Neuroscience, Computational Neuroscience Laboratories, Advanced Telecommunications Research Institute International (ATR), Kyoto, Japan. He is also the Group Leader for Japan Science and Technology Agency (JST), International Cooperative Research Project (ICORP), Computational Brain Project, Saitama, Japan. His current research interests include humanoid robotics, cognitive systems, biomimetic of human vision, computational neuroscience of vision, action understanding, human–robot interaction, active vision, mobile robot navigation, and object-oriented software construction. He is on the editorial board of the *International Journal of Humanoid Robotics*.

Dr. Cheng is a Senior Member of the IEEE Robotics and Automation Society and the IEEE Computer Society.